Low-temperature growth of polyethylene glycol-doped $BiZn_2VO_6$ nanocompounds with enhanced photoelectrochemical properties

Sami Elhag, Daniel Tordera, T Deydier, Jun Lu, Xianjie LiU, Volodymyr Khranovskyy, Lars Hultman, Magnus Willander, Magnus Jonsson and Omer Nur

Journal Article

Original Publication:

Sami Elhag, Daniel Tordera, T Deydier, Jun Lu, Xianjie LiU, Volodymyr Khranovskyy, Lars Hultman, Magnus Willander, Magnus Jonsson and Omer Nur, Low-temperature growth of polyethylene glycol-doped $BiZn_2VO_6$ nanocompounds with enhanced photoelectrochemical properties, Journal of Materials Chemistry A, 2017. (3), pp.112-1119.
http://dx.doi.org/10.1039/C6TA10180A

Low-temperature growth of polyethylene glycol-doped $BiZn_2VO_6$ nanocompounds with enhanced photoelectrochemical properties

S. Elhag, [*a] D. Tordera, [a] T. Deydier,[b] J. Lu,[c] X. Liu,[c] V. Khranovskyy,[c] L. Hultman,[c] M. Willander,[a] M. P. Jonsson,[a] and O. Nur. [a]

Abstract

We demonstrate scalable, low-cost and low-temperature (<100 ^{O}C) aqueous chemical growth of bismuth-zinc vanadate ($BiZn_2VO_6$) nanocompounds by $BiVO_4$ growth on ZnO nanobelts (NBs). The nanocompounds were further doped with polyethylene glycol (PEG) to tune the electronic structure of the materials, as a means to lower the charge carrier recombination rate. Chemical composition, morphology, and detailed nanostructure of the $BiZn_2VO_6$ nanocompounds were characterized. They exhibit rice-like morphology, are highly dense on the substrate and possess a good crystalline quality. Photoelectrochemical characterization in 0.1 M lithium perchlorate in carbonate propylene shows that the $BiZn_2VO_6$ nanocompounds are highly suitable as anodes for solar-driven photoelectrochemical applications, providing significantly better performance compared with only the ZnO NBs. This performance could be attributed to the heterogeneous catalysis effect at nanocompounds and ZnO NBs interfaces, which have enhanced the electron transfer process on the electrode surface. Furthermore, the charge collection efficiency could be significantly improved through PEG doping of the nanocompounds. The photocurrent density for PEG-doped $BiZn_2VO_6$ nanocompounds reached values of 2 mA cm^{-2} at 1.23 V (vs Ag/AgCl), over 60% larger than that of the undoped $BiZn_2VO_6$ nanocompounds. Photoluminescence emission experiments confirmed that the PEG plays a crucial role in lowering the charge carrier recombination rate. The presented $BiZn_2VO_6$ are shown to provide highly competitive performance compared with other state-of-the art photoelectrodes.

Key words: Mixed metal oxide, bismuth-zinc vanadate, low temperature aqueous chemical growth, doping and enhanced photoelectrochemistry water oxidation.

1. Introduction

Nanostructured semiconductors have great potential to be used as photocatalytic electrodes for photoelectrochemical (PEC) applications like water splitting and pollutant degradation. In addition to strong light absorption and efficient charge separation/migration of photogenerated charges, suitable PEC electrodes should also provide low recombination rates and efficient charge separation/migration, while remaining stable.[1-3] However, the semiconductor electrodes must also be compatible with scalable low-cost synthesis. Some single phase metal oxide (MO) nanostructures (e.g. CuO, ZnO, TiO_2, Fe_2O_3[4-6)] are promising as photo-electrode materials for visible light induced photo-catalysis because of their high catalytic properties along with their chemical, structural, and electronic surface composition that can be tailored with specific properties. However, to date, no single phase material exists that can be used to meet all the aforementioned demands. Previous efforts to improve these properties of photoelectrodes include doping of the semiconductor and modification of the electrode surface with water oxidation co-catalysts,[7-11] and development of novel photo-catalysts such as $BaTaO_2N$,[12] $BiPO_4/BiVO_4$,[13] Bi_2MoO_6/ZnO,[14] GaN:ZnO (oxynitride)[15] and graphitic carbon nitride (g-C_3N_4).[16]

Mixed metal oxides in the form BiM_2AO_6 (with M: Mg, Ca, Cd, Cu, Pb, Mn or Zn, and A: V, P or As) possess suitable physical and chemical properties for PEC water oxidation.[17-20] However, only a few candidates have been investigated, namely $BiCu_2VO_6$[18] and $BiZn_2VO_6$.[19,20] Particularly, bismuth zinc vanadate ($BiZn_2VO_6$) presents a band gap (E_g) in the visible wavelength range, with measured and calculated reported values of around 2.4 eV[19] and 1.6 eV,[17] respectively. By contrast, ZnO has a E_g of around 3.3 eV and can only absorb the ultraviolet part (<5%) of the solar spectrum.[2] Effectively, $BiZn_2VO_6$ merges the most suitable properties from the two individual components, ZnO and $BiVO_4$. This means that it acts as a robust visible light absorber (originating from the $BiVO_4$, while a limitation of ZnO), while also providing a high electron mobility to facilitate efficient charge transport (originating from the ZnO, while a limitation of $BiVO_4$).[9,10] In addition, charge transport properties of this combination may be improved by doping with polyethylene glycol (PEG), as we recently demonstrated for ZnO nanorods.[21] The water-PEG solution acts as an impurity source by the disruption of hydrogen bonding when dissolved in water and also provides a rich hydrogenated environment for the growth of

ZnO nanorods. The obtained doping density ($1.39 \cdot 10^{20}$ cm^{-3}) extracted from Mott-Schottky analysis for PEG-doped ZnO was higher than for the undoped ZnO ($2.81 \cdot 10^{19}$ cm^{-3}), with associated enhanced optical and sensing properties.[21]

Scalable, low-cost and environmentally friendly synthesis is essential for practical applications. To date all the grown BiM_2AO_6 compounds[16-19] were to our knowledge prepared for growth durations in excess of 10 h and by high-temperature (≥ 700 °C) solid-state reactions. This render them expensive and does not allow neither a doping using an organic compound nor the utilization of soft substrates. Instead, aqueous chemical growth (ACG), "green chemistry", is a low-temperature method for production of metal oxide nanostructures.[22,23] In addition to the low cost of this synthesis route, ACG can be operated at sufficiently low-temperatures (< 100 °C) to allow organic molecules to be used as additives as a means to control the nanostructure morphology.[21]

In this report, for the first time, an inexpensive, scalable, and low temperature (80-90 °C) green synthesis of $BiZn_2VO_6$ nanocompounds (NCs), by $BiVO_4$ growth on ZnO nanobelts(NBs)-based modified electrodes. The PEC properties of the NCs were characterized and further enhanced by PEG-doping. The $BiZn_2VO_6$ NCs are characterized by X-ray diffraction (XRD), high-resolution transmission electron microscopy (HRTEM), X-ray photoelectron spectroscopy (XPS), and scanning electron microscopy (SEM) techniques. Furthermore, we compare the PEC properties of four different type of electrodes (pristine ZnO NBs, PEG-doped ZnO NBs, pristine $BiZn_2VO_6$, and PEG-doped $BiZn_2VO_6$) under a simulated solar irradiation (AM1.5G). photocurrent density of the pristine $BiZn_2VO_6$ --NCs was up to ~1.25 mA cm-2 at 1.23 V vs Ag/AgCl, while the PEG-doped $BiZn_2VO_6$ NCs reached values of ~ 2 mA cm^{-2} at 1.23 V vs Ag/AgCl for the same experimental conditions, nearly 61.5% larger than that of the pristine $BiZn_2VO_6$ NCs. Photoluminescence (PL) emission studies show that the PEG plays a crucial role in lowering the charge carrier recombination rate.

2. **Experimental section**

2.1. **Synthesis of the $BiZn_2VO_6$ nanocompounds**

The $BiZn_2VO_6$ compound nanostructures were prepared by a two-step low-temperature aqueous chemical growth (ACG) process as showed in Scheme 1. Firstly, pristine and doped ZnO nanorods were prepared over an Au-coated glass, as previously

reported.[21] Briefly, the growth solution used in this experiment was prepared from an equimolar concentration of 0.05 M solutions of zinc nitrate hexahydrate $ZnNO_3 \cdot 6H_2O$ and hexamethylenetetramine $C_6H_{12}N_4$ in deionized water. For doped samples, the growth was also in the presence of 0.1% weight to volume (w/v) polyethylene glycol (PEG, molecular weight 2000). The substrates were fixed facing downwards to a Teflon sample holder and then dipped into the growth solution. After that they were baked in an oven for 5 h at 90 °C. After the growth time was completed, the samples were washed in deionized water and dried with nitrogen gas (Scheme 1a). In the next step, the $BiZn_2VO_6$ compound was formed by $BiVO_4$ growth on top of the ZnO nanostructure, according to Zhou's and co-workers report albeit at modified growth time.[24] In a typical synthetic route, equimolar concentration of 0.02 M of bismuth(III) nitrate pentahydrate ($Bi(NO_3)_3 \cdot 5H_2O$) and ammonium metavanadate (NH_4VO_3) were dissolved in 10 mL of nitric acid, 70% (HNO_3) solution. 20 ml deionized water was added into this solution under vigorous stirring until the salts were completely dissolved. Then, ~12.8 g sodium hydrogen carbonate ($NaHCO_3$) was added to adjust the pH value to 6.5 until the formation of a yellow homogeneous solution. The as-grown ZnO nanorods on Au-coated glass were placed facing upwards in the bottom of this yellow solution. They were covered with aluminum foil and placed in the pre-heated oven for 4 or 10 h at 80 °C. The final products were washed with deionized water, dried with nitrogen gas and then dried at 80 °C for 10 h in the oven (Scheme 1b).
ZnO samples were used as reference for the photoelectrochemical characterization. As the concentration of alkaline reactant has a direct effect on the pH of growth solution,[23] in order to have the same ZnO morphology (ZnO nanobelts (NBs)) as the aforementioned synthetic route, the as-prepared pristine and doped ZnO nanorods electrodes were immersed in a solution containing 10 ml of nitric acid, 70% HNO_3, and 20 ml deionized water. $NaHCO_3$ was added to adjust the pH value to 6.5 and then the samples were placed in an oven for 4 h at 80 °C. Also $BiVO_4$ control samples for XRD, and XPS measurements were grown on Au coated glass substrate as described above with an extra step for the seed solution. The seed solution was prepared by using an equimolar concentration of 0.02 M of bismuth(III) nitrate pentahydrate and ammonium metavanadate in 25 ml methanol. This seed solution was deposited on a cleaned Au coated glass substrates by the dip coating method. The substrates containing the seed particles were then annealed at 120 °C for 5 min. After preparing the substrates with seed nanoparticles, it was placed in the beaker containing the growth solution. They were covered with aluminum foil and

placed in the pre-heated oven for 4 h at 80 °C. The final products were washed with deionized water, dried with nitrogen gas and then dried at 80 °C for 10 h in the oven.

2.2. Characterization of the electrodes

The structural characterization was carried out by X-ray powder diffraction (XRD) using a Philips PW 1729 powder diffractometer equipped with a CuKα radiation source (λ=1.5418 Å) using a generator voltage of 40kV and a current of 40mA. The high-resolution transmission electron microscopy (HRTEM) characterization was carried out by using a FEI Tecnai G2 TF20 UT instrument with a field-emission gun operated at 200 kV. The instrument is equipped with an EDX system. Optical absorption spectra were obtained by a PerkinElmer Lambda 900 UV–visible spectrophotometer. $BiZn_2VO_6$ nanostructures grown on glass substrate were used for the measurements. A blank glass slide was used as a reference. Surface and chemical composition analysis were investigated by X-ray photoelectron spectroscopy (XPS) and were measured using a Scienta ESCA200 spectrometer with vacuum generators and monochromatic Al Kα radiation. Field emission scanning electron microscopy (SEM) for morphological analysis was performed by using a LEO 1550 Gemini field emission gun at 5kV. The optical properties were investigated by photoluminescence (PL) measurements at room temperature (300 K). The light emission features of the samples were studied by a micro-photoluminescence setup. Excitation was performed by a frequency doubled Nd:YVO laser as a continuous wave excitation source, with a wavelength λ = 266 nm.

2.3. Photoelectrochemical characterizations

The photoelectrochemical (PEC) measurements (linear sweep voltammetry (LSV)), chronoamperometry and electrochemical impedance spectroscopy (EIS)) were performed in a three-electrode cell setup using an SP-200 potentiostat (Bio-Logic, Claix, France), a platinum sheet as the counter electrode and a standard Ag/AgCl reference electrode in 3M KCl. The electrolyte used was 0.1 M Lithium perchlorate ($LiClO_4$) in propylene carbonate solution at pH 7 to avoid ZnO decomposition.[25] The LSV was carried out at a scan rate of 0.1 V/s. Chronoamperometry *I-t* curves were tested at a bias voltage of 0.5 V (vs Ag/AgCl). All electrodes were illuminated from the front side of the samples by a solar simulator (LCS-100, Newport, model 94011A). The total area of the photoelectrode was 2 cm x 1 cm, while the light is illuminated on a 1 cmx 1 cm that was

immersed in the electrolyte. The solar simulator uses a 100 W ozone free xenon lamp and includes an AM1.5G air mass filter with output power of 1 Sun (AM1.5G). The EIS was performed at an amplitude of 20 mV, in the frequency range of 5 kHz–0.1 Hz, and potential range of -1.0 V to +1.0 V.

3. Result and discussion

3.1. Characterization of the products

Fig. 1 shows XRD patterns of representative ZnO, PEG-doped ZnO, $BiVO_4$, $BiZn_2VO_6$, and PEG-doped $BiZn_2VO_6$ NCs grown by low-temperature ACG for 4 h and 10 h. The XRD acquisition parameters were kept the same for all samples to ensure a fair comparison between samples. The peak at $2\theta = 38°$ corresponds to the Au substrate and was observed for all samples. The XRD patterns of the pristine and the PEG-doped ZnO NBs show peaks corresponding to the (100), (002), and (101) planes of ZnO at $2\theta = 31.77°$, 34.42°, and 36.25°, respectively. This confirms that the ZnO NBs have a hexagonal wurtzite structure (JCPDS NO 36-1451). In agreement with our previous work on PEG-doped ZnO nanorods, PEG-doping does not significantly affect the structural properties of the ZnO NBs.[21] $BiVO_4$ is known to exist in three polymorphs: orthorhombic, tetragonal, and scheelite structure with monoclinic.[26] The XRD patterns of $BiVO_4$ monoclinic and tetragonal systems are quite similar, but $BiVO_4$ scheelite structure with monoclinic system can be distinguished by the existence of a 2θ peak at 15° and a peak splitting at 18.5°, 35°, and 46°.[27] All XRD results for the $BiVO_4$ control samples were in agreement with the characteristic pattern arising from the monoclinic scheelite phase (JCPDS NO 74-4894). The XRD patterns of the $BiZn_2VO_6$ NCs samples exhibit several peaks that cannot match any peak of pure ZnO or $BiVO_4$ samples. Comparing this with the XRD results of the work reported by S. E. Nunes *et al.*,[17] it is clear that the grown samples are not a ZnO/$BiVO_4$ composite, but rather bismuth zinc vanadate ($BiZn_2VO_6$). In fact, it is a mixed metal oxide NCs that crystallizes in orthorhombic unit cells.[17,28] Comparing the XRD results for $BiZn_2VO_6$ and PEG-doped $BiZn_2VO_6$ grown for 4 h and 10 h, we noticed that the XRD patterns are same for both samples *i.e.* no time and no PEG-doping dependence. Therefore, one can infer that 4 h is already a suitable growth time for the $BiZn_2VO_6$ NCs. This is an improvement compared to previous published results on the growth of $BiZn_2VO_6$ using high-temperature

solid-state reactions and relatively longer growth durations (≥ 700 °C, up to 30 h).[17-20] In order to further confirm that we have obtained a $BiZn_2VO_6$ NCs, a study was performed by HRTEM on the $BiVO_4$/doped ZnO/Au electrode that was prepared by 10 h synthesis. Selective area electron diffraction (SAED) pattern of a single NC (Fig. 2a) shows well-defined diffraction spots, indicating a polycrystalline nature of the NC. Furthermore, energy dispersive X-ray spectroscopy (EDX) mapping of the sample (Fig. 2b) demonstrates that the Zn distribution overlaps with the Bi and V distributions, which means that $BiVO_4$ is intertwined with doped ZnO, *i.e.* PEG-doped $BiZn_2VO_6$ NCs have been grown. Moreover, UV-Vis. spectroscopy was used as shown in Fig. 3. The absorption spectrum for $BiZn_2VO_6$ material grown on glass substrate indicates an absorption peak at around ~ 482 nm, which corresponds to an optical band gap of about 2.57 eV. This is larger than previously reported data[19] by 0.17 eV.

We also used XPS to analyse the chemical state of the PEG-doped $BiZn_2VO_6$ and the $BiVO_4$ control samples (Fig. 4a and 4b, respectively). For the $BiVO_4$ control samples (Fig. 4b), the O1s and $V2p_{3/2}$ XPS peaks at ~530 eV and ~516.8 eV correspond to the oxygen species in the metal oxide and vanadium oxide phase, respectively.[29] The strong shoulder of the O1s peak at ~ 532 eV might be due to the hydroxyl group from adsorbed water.[30] For the PEG-doped $BiZn_2VO_6$ NCs, the dominant feature in the O1s spectrum belong to the hydroxyl group and adsorbed water which gives a strong peak at ~ 532 eV. The contribution from oxygen species in O1s spectrum now appears as a tail in the lower binding energy (marked by a circle in Fig. 4a). It should also be noted that the $V2p_{3/2}$ XPS peak at ~ 517 eV shifts slightly to a higher binding energy (vertical reference line) for PEG-doped $BiZn_2VO_6$ compared to the pristine $BiVO_4$ sample. Furthermore, Bi4f XPS peaks for the PEG-doped $BiZn_2VO_6$ NCs were different from those of the pristine $BiVO_4$ as shown in Fig. 4c. The observed binding energies of Bi4f7/2 (159.3 eV) and Bi4f5/2 (164.9 eV) of the $BiVO_4$ are consistent with literature data.[29,31] In comparison, the peak positions of Bi4f7/2 (159.8 eV) and Bi4f5/2 (165.2 eV) for the $BiZn_2VO_6$ are shifted to higher binding energies. We note that, in our previous work[21] the presence of the PEG, caused the core level of the O1s to shift by ~ 0.4 eV to lower binding energy. However, in the current work the O1s was not affected and remained at the same value of the binding energy for the control $BiVO_4$ sample and doped $BiZn_2VO_6$, while the V2p, and Bi4f have been shifted to higher binding energy. At this point it's convenient to recall that, the unit cell of the monoclinic $BiVO_4$ has a~ 7.2 Å, b ~ 11.7 Å, and c ~ 5.1 Å,[29] while mixed metal

oxides (BiM_2AO_6) is orthorhombic and possesses a unit cell with a~11.5 Å, *b*~5.5 Å and *c*~8.5 Å.[17] Consequently, the bonding length and the band structure is expected to be different for $BiVO_4$ and $BiZn_2VO_6$. Hence, the shift in the binding energies are mainly attributed to the incorporation of ZnO element into the $BiVO_4$ structure. The Zn2p XPS spectra of the $BiZn_2VO_6$ is shown in Fig. 4d, where the spin-orbital splitting peaks at ~1022.3 and ~1045.4 eV are assigned to the $Zn2p_{3/2}$ and $Zn2p_{1/2}$, respectively.[21] Based on these observations and from the aforementioned TEM and XRD results, it is evident that we have obtained a $BiZn_2VO_6$ NCs.

In order to identify possible changes of the ZnO nanorods during $BiZn_2VO_6$ growth, we examined ZnO nanorods films that were exposed to a modified $BiZn_2VO_6$ growth solution not containing the actual growth material (see experimental section for details). Comparing Fig. 5a (initial ZnO nanorods) and Fig. 5b (post-treated films) there is a clear etching effect of the nanorods, reforming into nanobelts (NBs, Fig. 5b). The lengths of these ZnO NBs are about 3-5 μm, their average side thickness is around 100 nm, and their widths range between around 300 nm and 700 nm. The morphology of ZnO nanostructures is known to be sensitive to external conditions like pH,[20] and we attributed the observed morphological change to the lower pH of the $BiZn_2VO_6$ growth solution (pH ≈ 6.0–6.5) compared with the growth solution of the initial ZnO nanorods (pH ≈ 6.5 and 7). Fig. 5c and d show samples after growth of PEG-doped $BiZn_2VO_6$ NCs on the ZnO NBs, by ACG during 4 h and 10 h, respectively. The nanostructures grown on the ZnO have a rice-like shape, with average height of 1.3-1.8 μm and widths between 1.9 μm and 2.6 μm. As clearly seen on the SEM pictures, the agglomeration and the size of $BiZn_2VO_6$ capped ZnO NBs increase with increasing growth time. Side view SEM image of the $BiZn_2VO_6$/ZnO/Au film is displayed in Fig. 5e, where rice-like $BiZn_2VO_6$ nanostructures grown in 4 h lay at the top of vertically-aligned ordered ZnO NBs. Note that from the top-down SEM image (Fig. 5f), the agglomeration of $BiZn_2VO_6$ nanostructures at the top of the ZnO NBs is distributed randomly, while the cross-section image (Fig. 5e) reveals that $BiZn_2VO_6$ is interpenetrating the ZnO NBs. Both designs ensure close contact between the two components, which is highly desirable for charge transfer and separation.

3.2. Photoelectrochemical measurements

We investigated the PEC properties of pristine ZnO NBs, PEG-doped ZnO NBs, $BiZn_2VO_6$, and PEG-doped $BiZn_2VO_6$ electrodes under simulated solar light (see experimental section for details). Fig. 6a shows linear sweep voltammetry for all samples at dark conditions (dashed lines) and under light irradiation (full curves). First, we note that all four electrodes types provide considerable PEC conversion upon irradiation, while the dark currents are very low. However, the current densities vary by more than a factor 5 for the different samples. The observed photocurrent density was 0.35 mA cm^{-2} and 0.59 mA cm^{-2} for the undoped and the PEG-doped ZnO NBs at 1.23 V (vs Ag/AgCl), respectively. In comparison, the photocurrent density was 1.25 mA cm^{-2} at 1.23 V (vs Ag/AgCl) for the undoped $BiZn_2VO_6$ NCs. Hence, the photocurrent density of the $BiZn_2VO_6$ NCs, when compared with pristine and PEG-doped ZnO NBs, increases significantly, which can be assigned to efficient electro-catalytic surface activity of the $BiZn_2VO_6$ NCs under visible light irradiation.[19] It is also higher than the reported photocurrent for $BiCu_2VO_6$, and modified $BiZn_2VO_6$ (0.082 mA cm^{-2} at 1 V vs Ag/AgCl, and 0.0004 mA cm^{-2} at 0.6 V vs Ag/AgCl, respectively)[18,19] (see Table I for details). Moreover, the photocurrent density of the PEG-doped $BiZn_2VO_6$ NCs are substantially improved. PEG-doped $BiZn_2VO_6$ NCs reached values of 2 mA cm^{-2} at 1.23 V vs Ag/AgCl which corresponds to an improvement over 60% compared to pristine $BiZn_2VO_6$ NCs. We note that these values are higher than the reported photocurrent for other systems based on the same components, such as $BiVO_4$/Al-doped ZnO heterostructures (1.5 mA cm^{-2} at 1.23 V vs. RHE)[9]. The performance is also comparable to that of the triple junction (Co-Pi/$BiVO_4$ /ZnO, and CoO_x/NiO/$BiVO_4$), (3 mA cm^{-2} at 1.2 V vs RHE, and 2.5 mA cm^{-2} at 0.6 V vs RHE),[10,11] (see Table I for details). Table I summarizes the photocurrent density for recently reported for compounds, including state-of-the art heterostructure materials and the undoped/PEG-doped $BiZn_2VO_6$ electrodes presented in this article. The performance of additional photocatalyst materials can be found in the review by Su et al. [1] These results indicate that, the PEG assists the photo-excited electrons and holes to overcome the energy barrier (*e.g.*, the binding energy) and enhances the charge separation/migration processes of the $BiZn_2VO_6$ NCs electrode. Overall, the improved charge collection efficiency of the electrode surface can be attributed to: (1) the heterogeneous catalysis effect at the $BiZn_2VO_6$/ZnO NBs interfaces were enhanced, and the resulted electron communications processes on the electrode surface were efficient, and (2) PEG impurities that act as

shallow donor and enhance the n-type conductivity as it has been suggested in our previous work.[21] These results are also consistent with previous published studies,[7-9] where the authors argued that the doping plays distinct roles in enhancing photoactivity of semiconductor materials. The time responses of the undoped and doped electrodes were examined by chronoamperometry in the dark (light off) and under simulated solar light (light on) at an applied voltage of +0.5 V as shown in Fig. 6b. The space between each illumination cycle was ~ 50 s to enable investigation of the time response and the resetting of the photo-electrodes to reach it is equilibrium position. The stationary photocurrent density was 0.09 mA cm^{-2}, 0.13 mA cm^{-2}, 0.14 mA cm^{-2}, and 0.2 mA cm^{-2} for undoped ZnO NB, PEG-doped ZnO NB, undoped $BiZn_2VO_6$, and PEG-doped $BiZn_2VO_6$, respectively. These results confirm that the PEG-doped $BiZn_2VO_6$ NCs based electrode exhibited the highest current density, with a good reproducibility and stability. Moreover, all electrodes show very fast rise and decay times (around 0.1 s) as shown in Fig. 6 c and d (PEG-$BiZn_2VO_6$ electrodes), which is favorable for photoactivity.

The interface between electrolyte and electrodes of pristine and PEG-doped $BiZn_2VO_6$ NCs was investigated using the Mott-Schottky method, with the aim to relate the effect of PEG doping to the flat band potential (V_{fb}) of the semiconductor electrodes.[32] From the intercept (Fig. 7a), and at a selected frequency (~ 1 kHz), the extracted values for V_{fb} for using pristine and PEG-doped electrodes are ~ -0.90 V and ~ -0.96 V (vs Ag/AgCl), respectively. The 0.06 V shift to higher values upon doping suggests that a higher Fermi level (E_F) could be obtained by PEG doping. This shift of the E_F toward the conduction band edge (E_c) is expected and consistent with our previous studies.[21] In which we demonstrated that the addition of PEG into ZnO growth solution was attributed to hydrogen doping, and the doping density ($1.39 \cdot 10^{20}$ cm^{-3}) extracted from Mott-Schottky analysis for PEG-doped ZnO was higher than the undoped ZnO ($2.81 \cdot 10^{19}$ cm^{-3}) and accordingly the n-type conductivity of ZnO nanorods were enhanced. Moreover, this result is also in agreements with the recent work of Cooper et al.,[33] where they have reported an enhancement in the n-type conductivity of $BiVO_4$ due to hydrogen treatment.

The PEC activity has a direct relation with electron-hole recombination rate, where lower recombination rate corresponds to higher PEC activity and vice versa.[10,12] In order to further elucidate the mechanism responsible for the PEC enhancement, room temperature photoluminescence (PL) spectra were recorded for both pristine and PEG-doped $BiZn_2VO_6$ NCs (Fig. 7b). Overall, the edge emission, due to free excitonic emission,

and the "green-yellow" band, called the deep level emission band centered at ≈ 590 nm.[35] It is obvious that the emission intensity of PEG-doped $BiZn_2VO_6$ NCs has greatly decreased, by about 50%, with respect to pristine $BiZn_2VO_6$ NCs, indicating that the PEG doping plays a crucial role in quenching the PL emission. This observation may be related to the intramolecular hydrogen bonds, because of the addition of PEG that provides a hydrogen rich environment[21], which can modulate the PL characteristic as Yang *et. al.*, reported.[36] They reported that, the PL of carbon nanodots is quenched at pH =1 because of the formation of intramolecular hydrogen bonds among the oxygen-containing surface groups. The reduction in the emission intensity here can be explained as follows: upon excitation, the carriers aim to recombine radiatively by emitting a photon with energy close to the near band edge emission or alternatively through deep level emission. At this point, it is convenient to recall that, although as pointed out above, hydrogen acts a shallow donor. However, hydrogen is amphoteric *i.e.,* can act as either a donor (H^+) or an acceptor (H^-). [37] Therefore, one could ascribe the effect of the PEG as a duel effect: one is in enhancing the conductivity and the other is surface passivation/stabilization of the electrons or holes at the semiconductor surface.[38] On the basis of the results of the Mott–Schottky and PL measurements, there is a possible modulation in the Fermi level (E_F) and recombination for the $BiZn_2VO_6$ electrode – electrolyte interface. Fig. 7c, shows the Fermi level (E_F) of the un-doped $BiZn_2VO_6$ while, in Fig. 7d of the PEG-doped $BiZn_2VO_6$ the Fermi level is shifted towards the conduction band (E_c).

Conclusions

In summary, we demonstrated a low-cost and scalable low temperature ACG method to synthesize $BiZn_2VO_6$ NCs on ZnO NBs on Au-coated glass substrates. Characterization of the morphology and the chemical composition of the NCs show that $BiVO_4$ growth on the ZnO rods lead to $BiZn_2VO_6$ NCs with rice-like morphology. The ZnO nanorods reformed to ZnO NBs during this process. The rice-like $BiZn_2VO_6$ were successfully used as photoelectrode for PEC activity in 0.1 M lithium perchlorate in carbonate propylene under simulated solar light. The results show a performance of 1.25 mA cm^{-2} at 1.23 V for the $BiZn_2VO_6$ NCs, which is an improvement of 28% compared with the ZnO NBs samples. The charge collection efficiency of the device was further enhanced through doping by PEG. The photocurrent density for PEG-doped $BiZn_2VO_6$ NCs s reached values of up to 2 mA cm^{-2} at 1.23 V (vs Ag/AgCl) under the same experimental conditions.

This is over 60% higher than that of the undoped $BiZn_2VO_6$ NCs and more than a factor 5 higher than for the undoped ZnO NBs electrodes. Moreover, the improved photocatalytic performance upon PEG-doping was in agreement with photoluminescence measurements, which revealed that PEG-doping had a crucial role in lowering the charge carrier recombination rate. The enhanced photo-activity of the modified $BiZn_2VO_6$ NCs electrodes is attributed to impurities on the metal oxide that is dictated by the used of PEG along with the heterogeneous catalysis effect at the $BiZn_2VO_6$/doped-ZnO NB interfaces result in efficient electron communications processes on the electrode surface. The low-cost and scalable synthesis combined with the doping of the mixed metal oxides opens a new route for efficient and cheap materials for many applications, including PEC water splitting.

Acknowledgements

This work was supported by Ministry of Higher Education and Scientific Research (Grant No. 700 for the year 2012), Khartoum-Sudan, the Wenner-Gren Foundations, the Swedish Government Strategic Research Area in Materials Science on Functional Material at Linköping University (Faculty Grant SFO-Mat-LIU No 2009 00971), the Swedish Foundation for Strategic Research, the ÅForsk Foundation, and the Swedish Research Council.

Notes and references

1 J. Su and L. Vayssieres, *ACS Energy Lett.,* 2016**,** ***1***, 121.

2 X. Chen, S. Shen, L. Guo, and S. S. Mao, *Chem. Rev*., 2010, **110**, 6503.

3 J. S. Lee, *Catal Surv Asia*, 2005, **9**, 217.

4 P. Basnet and Y. Zhao, *Catal. Sci. Technol.*, 2016, **6**, 2228.

5 A. Paracchino, V. Laporte, K. Sivula, M. Grätzel and E. Thimsen, *Nature Materials*, 2011, **10**, 456-461.

6 S. P. Berglund, F. F. Abdi, P. Bogdanoff, A. Chemseddine, D. Friedrich, and R. v. d. Krol, *Chem. Mater*. 2016, **28**, 4231.

7 L. Chen, F. M. Toma, J. K. Cooper, A. Lyon, Y. Lin, I. D. Sharp, and J. W. Ager, *ChemSusChem*, 2015, **8**,1066.

8 O. Zandi, B. M. Klahr and T. W. Hamann, *Energy Environ. Sci*., 2013, **6**, 634.

9 L. Zhang, E. Reisner, and J. J. Baumberg, *Energy Environ. Sci*., 2014, **7**, 1402.

10 S. J. A. Moniz, J. Zhu, and J. Tang, *Adv. Energy Mater*., 2014, **4**, 1301590.

11 M. Zhong, T. Hisatomi, Y. Kuang, J. Zhao, M. Liu, A. Iwase, Q. Jia, H. Nishiyama, T. Minegishi, M. Nakabayashi, N. Shibata, R. Niishiro, C. Katayama, H. Shibano, M. Katayama, A. Kudo, T. Yamada, and K. Domen, *J. Am. Chem. Soc.*, **2015**, ***137*** ,5053.

12 M. Hojamberdiev, E. Zahedi, E. Nurlaela, K. Kawashima, K. Yubuta, M. Nakayama, H. Wagata, T. Minegishi, K. Domen and K. Teshima, *J. Mater. Chem. A*, 2016**, 4**, 12807.

13 S. Wu, H. Zheng, Y. Lian, Y. Wu, *Mat. Res. Bulletin,* 2013, **48,** 2901.

14 B. Jin, Z. Jiao and Y. Bi, *J. Mater. Chem. A,* 2015**, 3**, 19702.

15 T. Takata, C. Pan and K. Domen, *Sci. Technol. Adv. Mater*., 2015, **16** 033506.

16 W.-J. Ong, L.-Ll. Tan, Y. H. Ng, S.-T. Yong, and S.-P. Chai, *Chem. Rev.*, 2016**, *116***, 7159., Z. Mo, X. She, Y. Li, L. Liu, L. Huang, Z. Chen, Q. Zhang, H. Xu, and H. Li, *RSC Adv.,* 2015, **5**, 101552.

17 S. E. Nunes, C.-H. Wang, K. So, J. S. O. Evans, I. R. Evans, *J. Solid Stat Chem.* 2015, **222**, 12.

18 H. Liu, R. Nakamura, and Y. Nakato, *ChemPhysChem*, 2005, **6**, 2499.

19 H Liu, R. Nakamura, Y. Nakato, *Electrochem. Solid-State Lett*., 2006, **9**, G187.

20 Y. Murakami, M. Ikarashi, M. Hashizume, A. Y. Nosaka, and Y. Nosaka, *Electrochem. Solid-State Lett.,* 2008*,* **11**, H42.

21 S. Elhag, K. Khun, V. Khranovskyy, X. Liu, M. Willander, O. Nur, Sensor, 2016, **16**, 222.

22 L. Vayssieres, *Adv. Mat.*, 2003, **15**, 464.

23 S. Elhag, Z. H. Ibupoto, V. Khranovskyy, M. Willander, and O. Nur, Vacuum 2015, **116**, 21.

24 Lin Zhou, Wenzhong Wang, and Haolan Xu, *Cryst. Growth Des.***, 2008**, ***8***, 728.

25 I. M.-Seró, F. F.-Santiago, B. Denier, and J. Bisquert, R. T.-Zaera, J. Elias, and C. L.-Clément, *App. Phys.Lett.*, 2006. **89**, 203117.

26 A. Walsh, Y. Yan, M. N. Huda, M. M. Al-Jassim, and S.-H. Wei, *Chem. Mater*., 2009, **21**, 547–551.

27 S. Tokunaga, H. Kato, and A. Kudo, *Chem. Mater*. 2001, **13**, 4624.

28 J. Huang, and A. W. Sleight, *J. Solid Stat. Chem.,* 1992, **100**, 170.

29 J. K. Cooper, S. Gul, F. M. Toma, L. Chen, P.-A. Glans, J. Guo, J. W. Ager, J. Yano, I. D. Sharp, *Chem. Mater.* 2014, **26**, 5365.

30 M. C. Biesingera, B. P. Paynec, A. P. Grosvenord, L. W.M. Laua, A. R. Gerson, R. St. C. Smart, Appl. Sur. Sci., 2011, **257**, 2717.

31Qingxin Jiaa, Katsuya Iwashinaa, and Akihiko Kudoa**,** Proc Natl Acad Sci. 2012, **109**, 11564.

32 K. Rajeshwar, Encyclopedia of electrochemistry: semiconductor electrodes and photoelectrochemistry; Licht, S., Ed.; Wiley-VCH: Weinheim, Germany, 2002; Chapter 1, pp. 1–53.

33 J. K. Cooper, S. B. Scott, Y. Ling, J. Yang, S. Hao, Y. Li, F. M. Toma, M. Stutzmann, K. V. Lakshmi, and I. D. Sharp, *Chem. Mater.*, **2016**, *28*, 5761.

34 A. B. Djurišić and Y. H. Leung, *Small*, 2006, **2**, 944.

35 V. Khranovskyy, V. Lazorenko, G. Lashkarev and R. Yakimova, *J. Luminescence*, 2012, **132**, 2643.

36 P. Yang, J. Zhao, L. Zhang, L. Li, and Z. Zhu, *Chem. Eur. J.,* 2015, **21**, 8561.

37 C. G. Van de Walle, and J. Neugebauer, *Nature*, 2003, **423**, 626.

38 J. M. Lauerhaas, M. J. Sailor, *Science*, 1993, **261,** 1567.

Figure captions

Scheme 1: Growth process of (a) ZnO nanorods and (b) $BiZn_2VO_6$ NCs.

Figure 1: (a) XRD patterns of ZnO NBs, PEG-doped ZnO NBs, $BiVO_4$, $BiZn_2VO_6$, and PEG-doped $BiZn_2VO_6$ NCs grown by low-temperature ACG during 4 h and 10 h.

Figure 2: (a) TEM image of a $BiZn_2VO_6$ and the inset corresponding SAED pattern. (b) EDX mapping exhibiting Bi, Zn, and V distribution.

Figure 3: UV-Vis. absorption spectrum of $BiZn_2VO_6$ grown on glass with the same procedure that on gold coated glass.

Figure 4: XPS study of the as grown $BiVO_4$ and PEG-doped $BiZn_2VO_6$ NCs on Au coated glass (a) and (b) O1s and V2p of $BiVO_4$ and PEG-doped $BiZn_2VO_6$ NCs, respectively. (c) Bi4f and (d) Zn2p spectra for $BiZn_2VO_6$ NCs.

Figure 5: SEM of (a) and (b) PEG-doped ZnO nanorods and ZnO NBs, respectively. (c) and (d) PEG-doped $BiZn_2VO_6$ NCs grown in 4 and 10 h, respectively. (e) zoom in of (d), and (g) side view of (d).

Figure 6: (a) Linear sweep voltammetry of ZnO NBs, PEG-doped ZnO NBs, $BiZn_2VO_6$ and PEG-doped $BiZn_2VO_6$ NCs electrodes in the dark and under solar light illumination (1 Sun), (b) Chronoamperometry *I–t* curves of all electrodes at an applied voltage of +0.5 V with 50 s light on/off cycles, (c) & (d) the enlarged response time of the PEG-$BiZn_2VO_6$ photoelectodes for the rise and the decay times of ~ 0.1s, respectively

Figure 7: (a) Mott–Schottky plots for pristine and doped $BiZn_2VO_6$ NCs electrodes in 0.1 M Lithium perchlorate ($LiClO_4$) in carbonate propylene (at the normal laboratory light conditions) at 1 kHz. (b) PL intensities normalized at 380nm spectra of the as-grown $BiZn_2VO_6$ and PEG-doped $BiZn_2VO_6$ NCs on gold-coated glass using a laser with a wavelength of 266 nm. (c) and (d) Schematic illustration of how PEG can affect the Fermi level (E_F) of the optical band gap of (c) pristine $BiZn_2VO_6$ and (d) PEG-doped $BiZn_2VO_6$ before equilibration at the electrolyte interface (E_F, redox).

Table I: Characteristics of $BiZn_2VO_6$ and doped $BiZn_2VO_6$ along with those reported in some literature for other compounds and heterostructure materials. RHE and SCE refer to reversible hydrogen electrode and saturated calomel electrode respectively.

Scheme 1

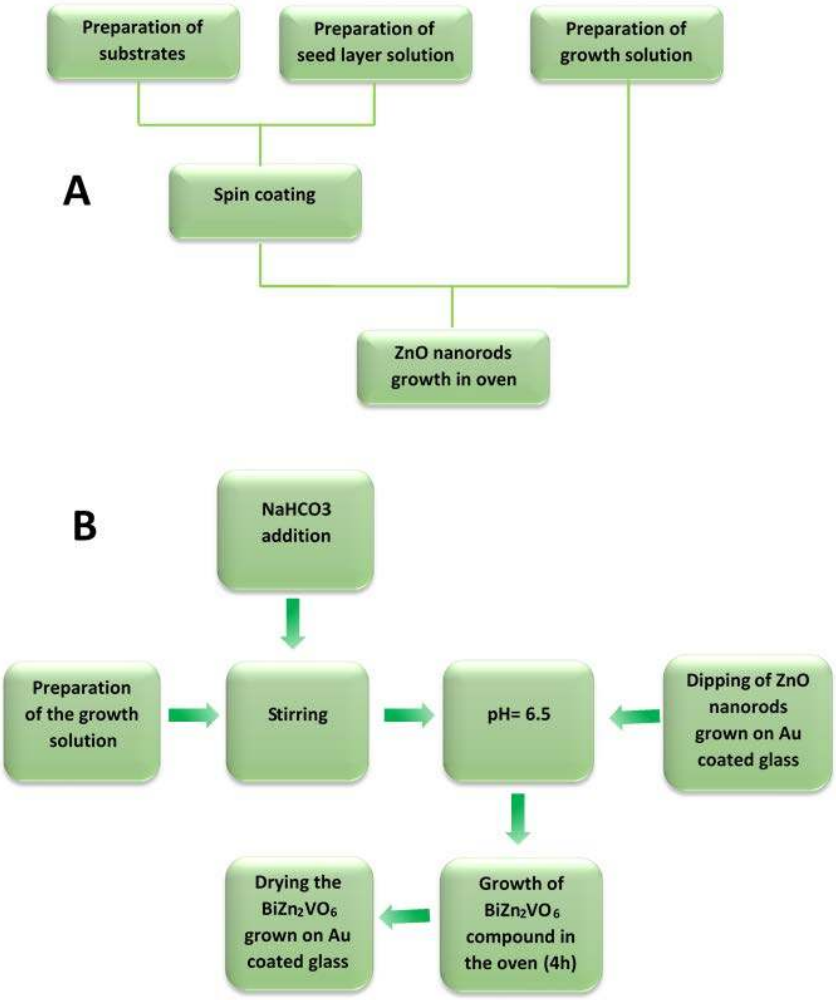
Preparation of substrates
Preparation of seed layer solution
Preparation of growth solution
A
Spin coating
ZnO nanorods growth in oven
B
NaHCO3 addition
Preparation of the growth solution
Stirring
pH= 6.5
Dipping of ZnO nanorods grown on Au coated glass
Growth of $BiZn_2VO_6$ compound in the oven (4h)
Drying the $BiZn_2VO_6$ grown on Au coated glass

Fig. 1:

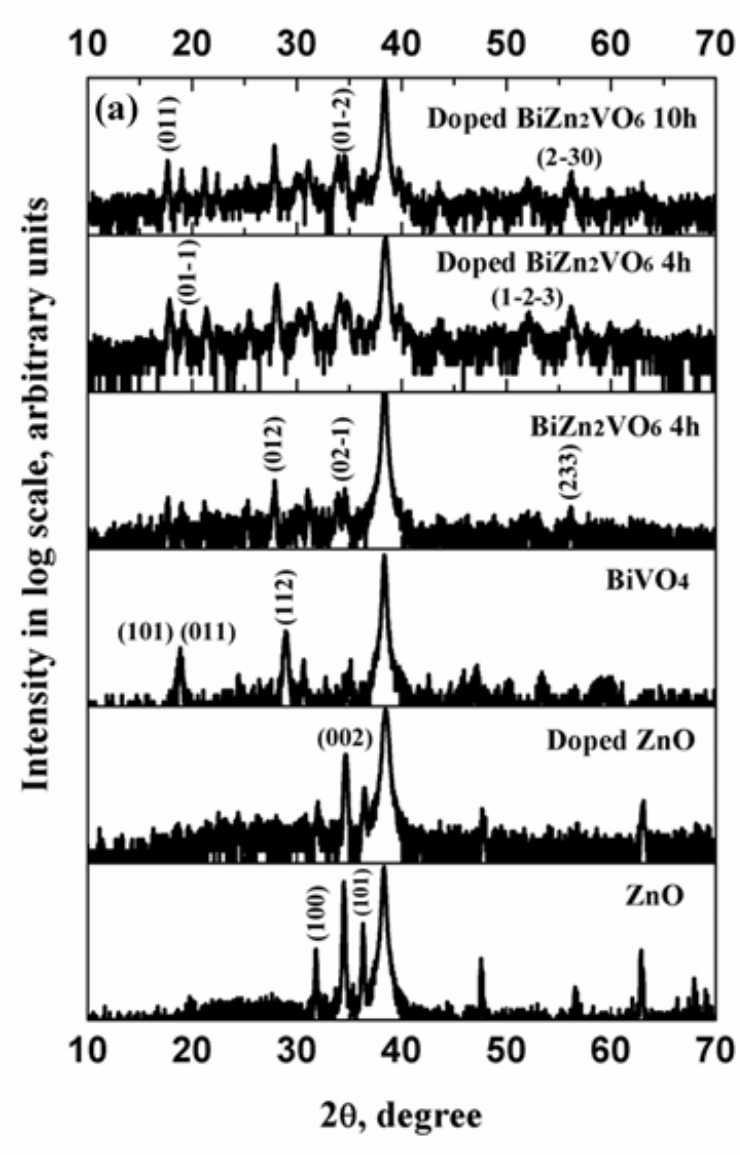
10
20
30
40
50
60
70
(a)
(011)
(01-2)
Doped BiZn2VO6 10h
(2-30)
(01-1)
Doped BiZn2VO6 4h
(1-2-3)
(012)
(02-1)
BiZn2VO6 4h
(233)
BiVO4
(101)
(011)
(112)
(002)
Doped ZnO
(100)
(101)
ZnO
Intensity in log scale, arbitrary units
2θ, degree

Fig. 2:

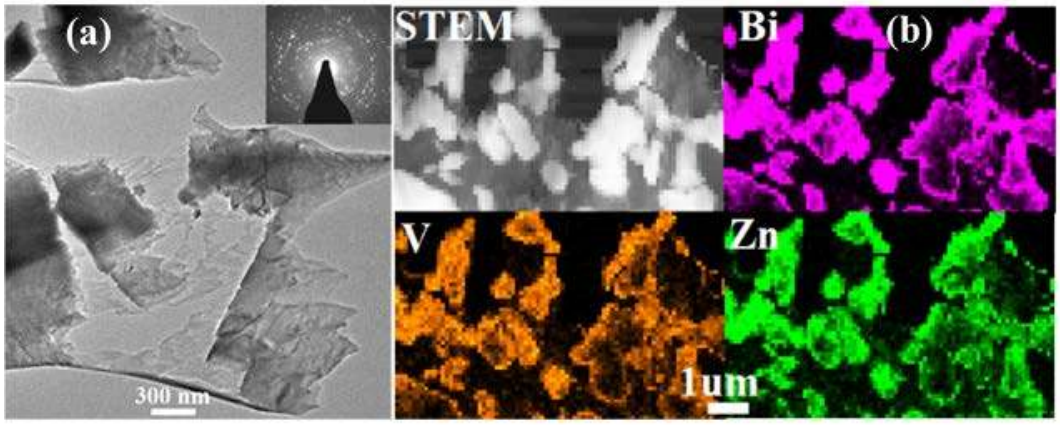

Fig. 3:

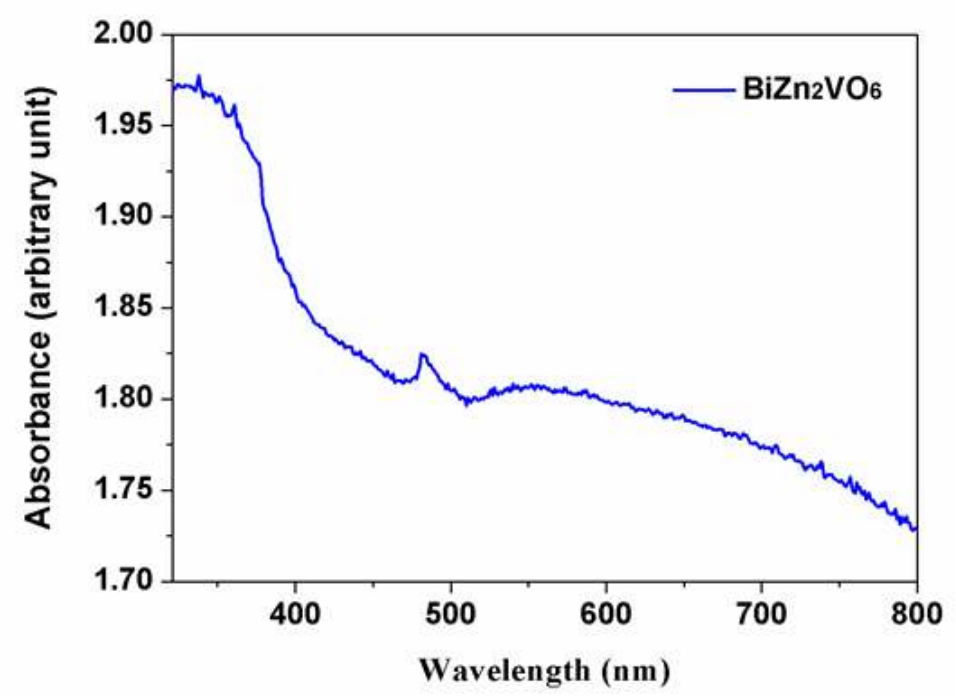
BiZn2VO6
Absorbance (arbitrary unit)
Wavelength (nm)
2.00
1.95
1.90
1.85
1.80
1.75
1.70
400
500
600
700
800

Fig. 4:

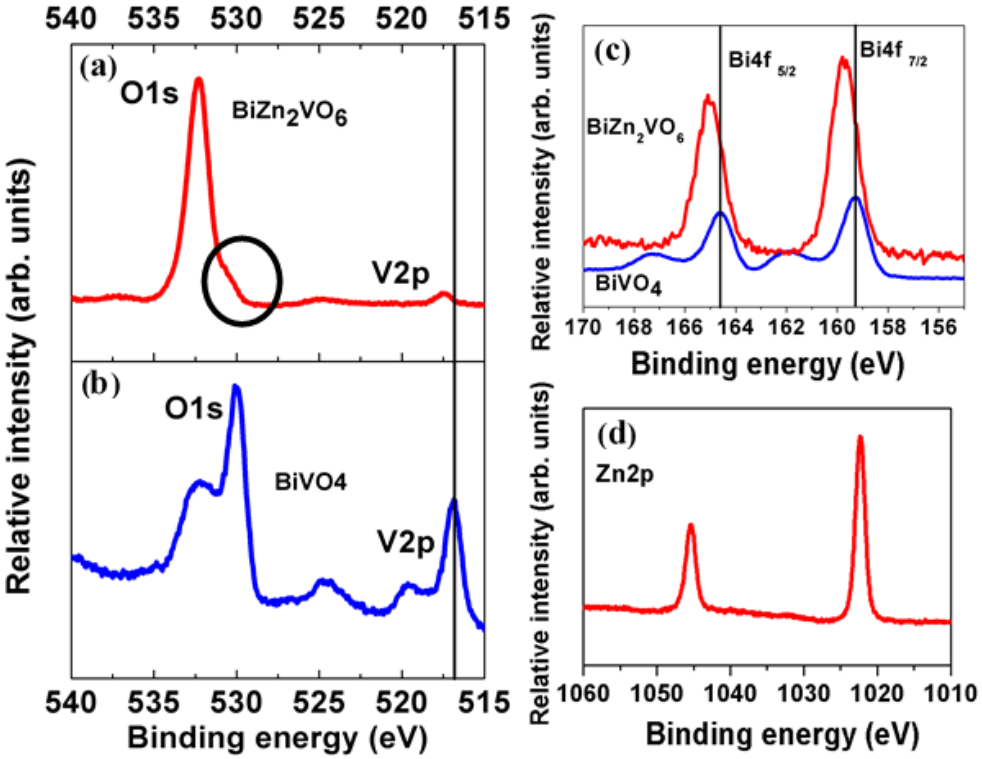
(a)
O1s
BiZn2VO6
V2p
(b)
O1s
BiVO4
V2p
Relative intensity (arb. units)
540 535 530 525 520 515
Binding energy (eV)
(c)
Bi4f 5/2
Bi4f 7/2
BiZn2VO6
BiVO4
Relative intensity (arb. units)
170 168 166 164 162 160 158 156
Binding energy (eV)
(d)
Zn2p
Relative intensity (arb. units)
1060 1050 1040 1030 1020 1010
Binding energy (eV)

Fig. 5:

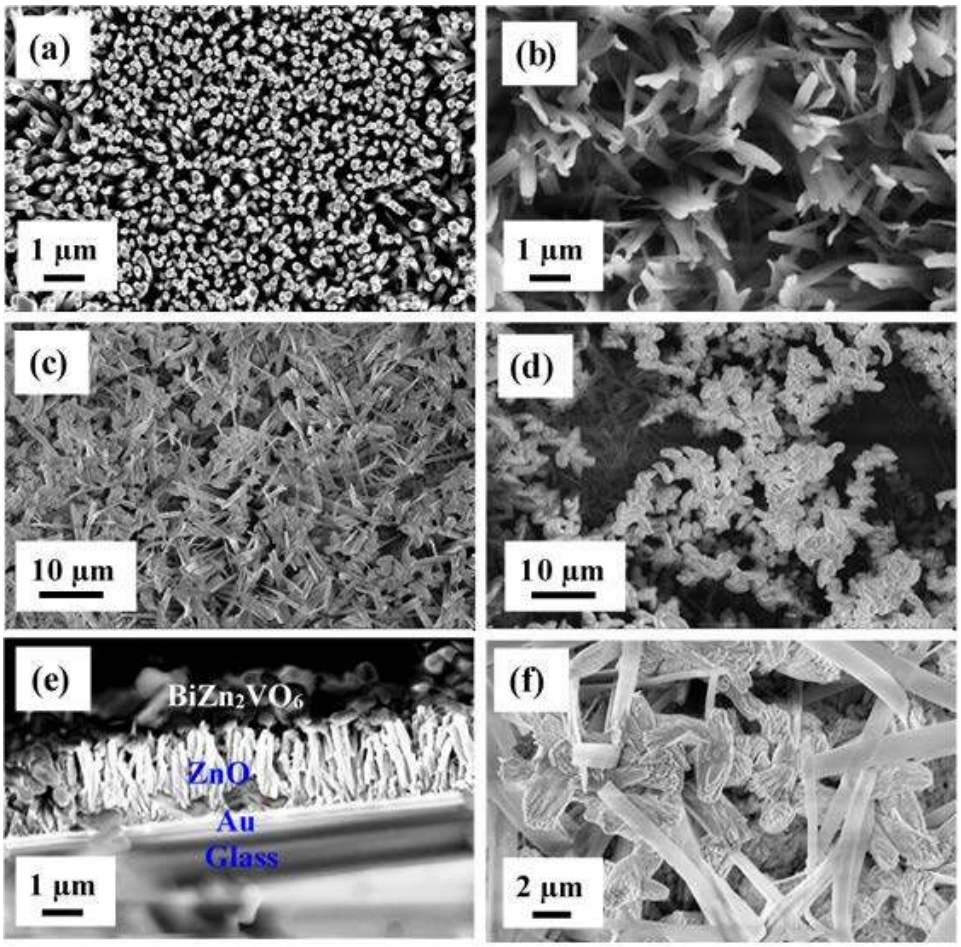

Fig. 6

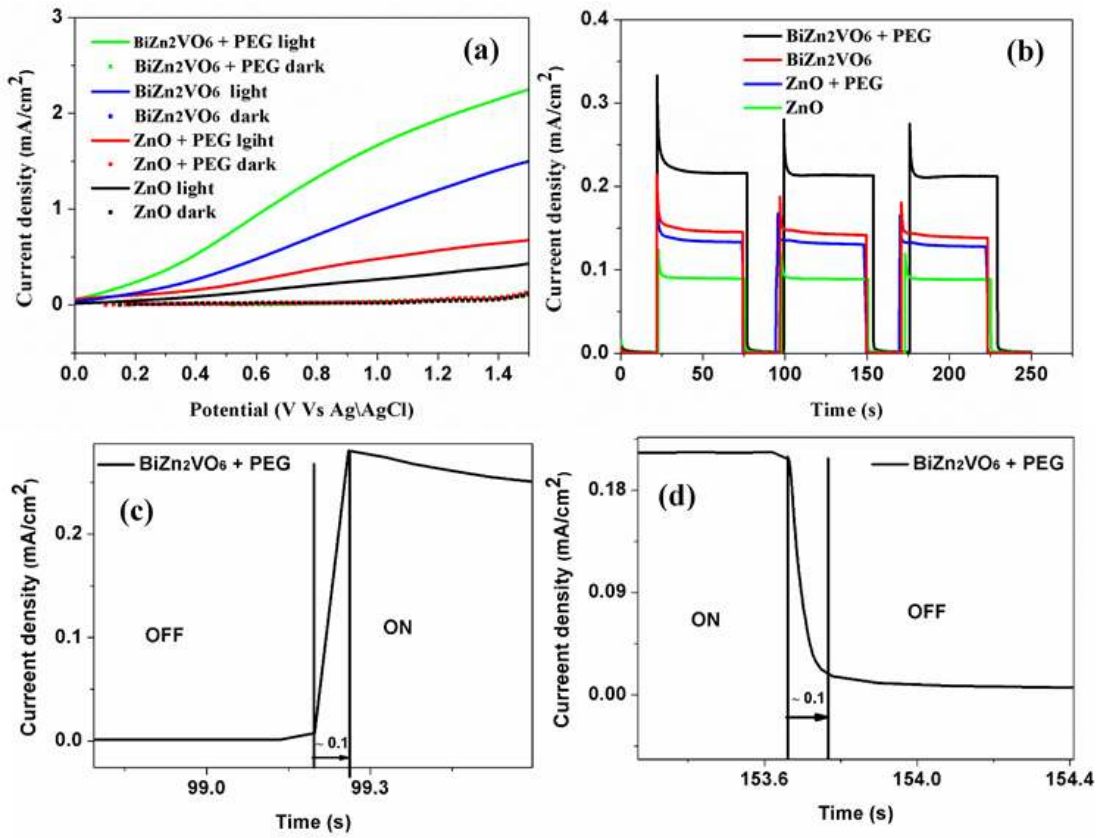
(a)
BiZn2VO6 + PEG light
BiZn2VO6 + PEG dark
BiZn2VO6 light
BiZn2VO6 dark
ZnO + PEG lgiht
ZnO + PEG dark
ZnO light
ZnO dark
Current density (mA/cm2)
Potential (V Vs Ag\AgCl)
(b)
BiZn2VO6 + PEG
BiZn2VO6
ZnO + PEG
ZnO
Current density (mA/cm2)
Time (s)
(c)
BiZn2VO6 + PEG
OFF
ON
~ 0.1
Current density (mA/cm2)
Time (s)
(d)
BiZn2VO6 + PEG
ON
OFF
~ 0.1
Current density (mA/cm2)
Time (s)

Fig. 7

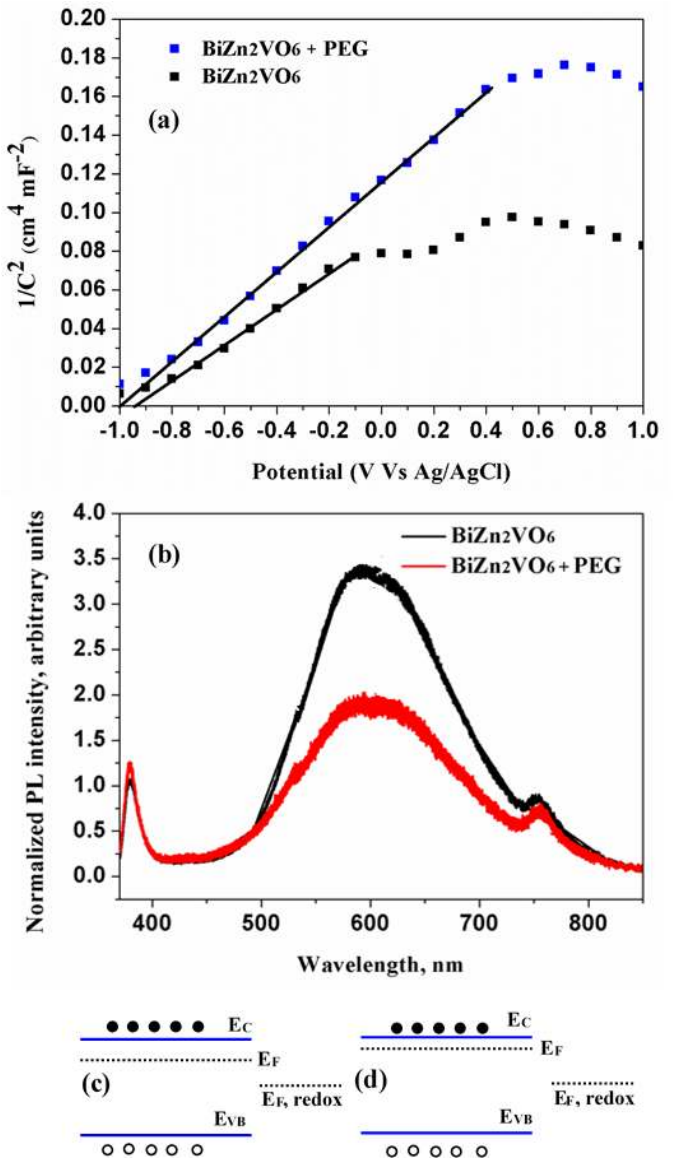
BiZn2VO6 + PEG
BiZn2VO6
(a)
1/C2 (cm4 mF-2)
Potential (V Vs Ag/AgCl)
BiZn2VO6
BiZn2VO6 + PEG
(b)
Normalized PL intensity, arbitrary units
Wavelength, nm
EC
EF
EF, redox
EVB
(c)
(d)

Table I:

Material	Condition	Performance
$BiZn_2VO_6$ NCs [this work]	0.1 M Lithium perchlorate in carbonate propylene (pH 7), AM 1.5G	1.25 mA cm^{-2} at 1.23 V vs Ag/AgCl
PEG-doped $BiZn_2VO_6$ NCs [this work]	0.1 M Lithium perchlorate in carbonate propylene (pH 7), AM 1.5G	2 mA cm^{-2} at 1.23 V vs Ag/AgCl
$BiZn_2VO_6$ (48-h etched by 0.5 M sulfuric acid) [20]	0.5M Na_2SO_4 (pH 6.4), 300-W Xe lamp (λ>420 nm)	0.4 μA cm^{-2} at 0.6 V vs Ag/AgCl
$BiCu_2VO_6$[18]	0.5M Na_2SO_4 (pH 6.4), AM 1.5G, 100 $mWcm^{-2}$	82 μA cm^{-2} at 1 V vs Ag/AgCl
$BaTaO_2N$ [12]	0.2 M K_2HPO_4 (pH 13), AM 1.5G 100 $mWcm^{-2}$	0.85 mA cm^{-2} at 1.2 Vs RHE
g-C_3N_4 [16]	0.1 M Na_2SO_4 500 W Xe arc lamp	1.2 μA cm^{-2} at −0.2 V *vs.* SCE
Bi_2MoO_6/ZnO [14]	0.2 M Na_2SO_4 (pH 7.0), 300 W Xe lamp, 100 mW cm^{-2}, (λ>420 nm)	110 μA cm^{-2} at 0.2 V vs. SCE
CoO_x/NiO/$BiVO_4$ [11]	0.1 M KPi, (pH 7) AM 1.5G	2.5 mA cm^{-2} at 0.6 V vs RHE
Co-Pi/$BiVO_4$ /ZnO[10]	0.2 M Na_2SO_4 (pH 6.5), AM 1.5G	3 mA cm^{-2} at 1.2 V vs RHE
$BiVO_4$/Al-doped ZnO [9]	phosphate buffer (pH 7), AM 1.5G (100 mW cm^{-2})	1.5 mA cm^{-2} at 1.23 V vs. RHE
Cu_2O and Cu_2O/CuO nanorods [4]	0.5 M Na_2SO_4 AM1.5G	0.06 mA cm^{-2} and 0.24 mA cm^{-2} respectively at −0.5 V vs. Ag/AgCl.